

Apparent local stability of the secondary structure of *Azotobacter vinelandii* holoflavodoxin II as probed by hydrogen exchange: Implications for redox potential regulation and flavodoxin folding

ELLES STEENSMA, MELANIE J.M. NIJMAN,¹ YVES J.M. BOLLEN, P. ADRIE DE JAGER,
WILLY A.M. VAN DEN BERG, WALTER M.A.M. VAN DONGEN, AND CARLO P.M. VAN MIERLO

Department of Biomolecular Sciences, Wageningen Agricultural University, Wageningen, The Netherlands

(RECEIVED June 26, 1997; ACCEPTED September 22, 1997)

Abstract

As a first step to determine the folding pathway of a protein with an α/β doubly wound topology, the ^1H , ^{13}C , and ^{15}N backbone chemical shifts of *Azotobacter vinelandii* holoflavodoxin II (179 residues) have been determined using multidimensional NMR spectroscopy. Its secondary structure is shown to contain a five-stranded parallel β -sheet ($\beta_2-\beta_3-\beta_1-\beta_4-\beta_5$) and five α -helices. Exchange rates for the individual amide protons of holoflavodoxin were determined using the hydrogen exchange method. The amide protons of 65 residues distributed throughout the structure of holoflavodoxin exchange slowly at pH* 6.2 ($k_{ex} < 10^{-5} \text{ s}^{-1}$) and can be used as probes in future folding studies. Measured exchange rates relate to apparent local free energies for transient opening. We propose that the amide protons in the core of holoflavodoxin only exchange by global unfolding of the apo state of the protein. The results obtained are discussed with respect to their implications for flavodoxin folding and for modulation of the flavin redox potential by the apoprotein. We do not find any evidence that *A. vinelandii* holoflavodoxin II is divided into two subdomains based on its amide proton exchange rates, as opposed to what is found for the structurally but not sequentially homologous α/β doubly wound protein Che Y.

Keywords: flavodoxin; hydrogen/deuterium exchange; NMR spectroscopy; protein folding; protein stability; redox potential regulation

We have chosen *Azotobacter vinelandii* (strain ATCC 478) flavodoxin II as a model protein to study protein folding. A flavodoxin was chosen because it adopts one of the nine protein domain superfolds (Orengo et al., 1994), the α/β doubly wound topology,

Reprint requests to: Carlo P.M. van Mierlo, Department of Biomolecular Sciences—Laboratory of Biochemistry, Wageningen Agricultural University, Dreijenlaan 3, NL-6703 HA Wageningen, The Netherlands; e-mail: carlo.vanmierlo@nmr.bc.wau.nl.

¹Present address: Laboratory of Biophysical Chemistry, University of Nijmegen, Nijmegen, The Netherlands.

Abbreviations: Amp, ampicillin; ct, constant-time; CSI, chemical shift index; DSS, 2,2-dimethyl-2-silapentane-5-sulfonate sodium salt; fid, free induction decay; ΔG_{op} , free energy for transient opening; ΔG_{op}^{app} , apparent free energy for transient opening in holoflavodoxin; ΔG_{unf} , equilibrium free energy of global unfolding; HSQC, heteronuclear single-quantum coherence; IPTG, isopropyl β -D-thiogalactopyranoside; k_{ex} , measured amide proton exchange rate; k_{int} , sequence-specific intrinsic amide proton exchange rate; K_d , dissociation constant; NOE, nuclear overhauser effect; NOESY, NOE spectroscopy; NMR, nuclear magnetic resonance; pH*, glass-electrode reading of the pH meter at room temperature, uncorrected for isotope effects; R, gas constant; t, time; T, temperature; TOCSY, total correlation spectroscopy; TPPI, time-proportional phase incrementation; TSP, 3-(trimethylsilyl)propionate sodium salt.

which consists of a five-stranded parallel β -sheet surrounded by α -helices at either side of the sheet (Fig. 1) (Ludwig & Luschinsky, 1992 and references therein). In addition, the good NMR characteristics of flavodoxins (solubility, relatively narrow linewidths) (van Mierlo et al., 1990b, 1997) will allow a detailed structural characterization of these proteins. NMR spectroscopy has proven to be particularly valuable to study protein folding. Native as well as non-native states of proteins can be studied using this technique (Shortle, 1996) and it has been demonstrated that hydrogen exchange pulse labeling methods in combination with NMR spectroscopy give detailed information about the folding pathways of proteins (Englander & Mayne, 1992; Woodward, 1994). In addition, recently it has become possible to follow protein folding in atomic detail by using “real time” NMR spectroscopy (Babach et al., 1995, 1996).

Flavodoxins are able to function as electron carriers between redox proteins because they contain a noncovalently bound FMN molecule (Mayhew & Tollin, 1992). *A. vinelandii* flavodoxin II (molecular mass 20 kDa) consists of 179 amino acid residues and belongs to the class of “long-chain” flavodoxins (Tanaka et al., 1977). When bound to the apoprotein, the FMN molecule can exist

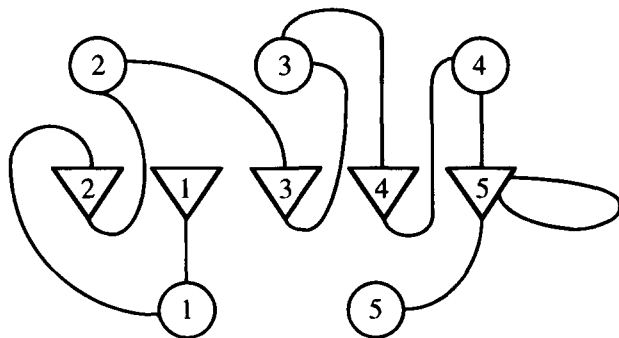
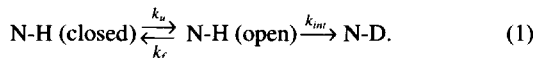


Fig. 1. Schematic drawing of the topology of long-chain flavodoxins. α -Helices are represented as circles, β -strands as triangles, and loops as lines. Note that a long loop (>20 residues) interrupts β -strand 5; this loop is absent in short-chain flavodoxins.

in three redox states: the oxidized flavoquinone, the one-electron reduced flavosemiquinone, and the two-electron reduced flavohydroquinone. We use in our studies the C69A mutant of *A. vinelandii* flavodoxin II in which the single cysteine has been replaced by an alanine to prevent complications due to intermolecular disulfide bridge formation (Steensma et al., 1996).

As a first, but crucial, step in the determination of the folding pathway of *A. vinelandii* holoflavinodoxin II using NMR spectroscopy, we report here its ^1H , ^{15}N , and ^{13}C backbone resonance assignments and its solution secondary structure. Three-dimensional triple resonance NMR studies were performed using both uniformly ^{15}N - and $^{15}\text{N}/^{13}\text{C}$ -labeled protein. Furthermore, we took advantage of the hydrogen exchange method in characterizing the apparent local stability of holoflavinodoxin. Here we demonstrate that 65 amide protons distributed throughout the structure of holoflavinodoxin exchange relatively slowly at pH* 6.2, $k_{ex} \leq 10^{-5} \text{ s}^{-1}$. This will enable us to perform hydrogen exchange pulse labeling experiments and to follow flavodoxin folding in great detail.

Hydrogen exchange rates can be analyzed in terms of a structural unfolding model, in which exchange only takes place from an “open” form of the protein, but not from the “closed” form (Linderstrøm-Lang, 1955; Hvidt & Nielsen, 1966; Englander & Kallenbach, 1984):



In this scheme, k_u and k_f are the local unfolding and folding rates, respectively, and k_{int} is the intrinsic exchange rate of an amide proton in the open form. The sequence-specific intrinsic exchange rates for an amide proton, k_{int} , can be calculated for each protein using the method of Bai et al. (1993). In the EX2 limit (bimolecular reaction), which is the dominant mechanism of exchange for most proteins at moderate pH and temperature, $k_f \gg k_u$ and $k_f \gg k_{int}$. Hence, the measured exchange rate, k_{ex} , can be written as:

$$k_{ex} = k_u * k_{int}/k_f = K_{op} * k_{int}, \quad (2)$$

where K_{op} is the equilibrium constant for local transient opening of a hydrogen bonded site. This equilibrium constant relates to ΔG_{op} , the structural free energy difference between the closed and open states:

$$\Delta G_{op} = -RT \ln K_{op} = -RT \ln(k_{ex}/k_{int}), \quad (3)$$

with R the gas constant and T the absolute temperature. One of the strengths of the hydrogen exchange method over equilibrium denaturation techniques lies in the capacity to pinpoint local differences in structural free energy. Furthermore, exchange of the most protected amide protons has been shown to often occur via global unfolding, in which case ΔG_{op} approximates ΔG_{unf} , the free energy of unfolding of a protein (Wagner & Wüthrich, 1979; Woodward, 1994; Jeng & Dyson, 1995; Englander et al., 1996).

However, in the case of holoflavinodoxin, the equilibrium with the apo state of the protein has to be considered:



in which the dissociation constant, K_d , is described by k_{off}/k_{on} . Unfortunately, this binding equilibrium complicates the interpretation of the hydrogen exchange data, because amide proton exchange can occur in either the holo- and/or the apoprotein. Because k_{off} is $4.8 \times 10^{-5} \text{ s}^{-1}$ and k_{on} is $1.1 \times 10^5 \text{ M}^{-1} \cdot \text{s}^{-1}$ (Pueyo et al., 1996), the observed exchange rate for a specific amide proton, k_{ex} , is the sum of the exchange rate of this particular proton in both the holo- and the apoprotein fraction:

$$\begin{aligned} k_{ex} &= f_{holo} * k_{ex}^{holo} + f_{apo} * k_{ex}^{apo}, \\ &= f_{holo} * K_{op}^{holo} * k_{int} + f_{apo} * K_{op}^{apo} * k_{int}, \end{aligned} \quad (5)$$

with f_{holo} and f_{apo} , the fractions holo- and apoflavinodoxin, respectively, that are present in the NMR sample, and k_{ex}^{holo} and k_{ex}^{apo} the amide proton exchange rate in the holo- and apoprotein, respectively. We report in this article the apparent local free energy of opening for the amide protons in holoflavinodoxin, according to:

$$\begin{aligned} \Delta G_{app}^{op} &= -RT \ln(k_{ex}/k_{int}) \\ &= -RT \ln\{f_{holo} * K_{op}^{holo} + f_{apo} * K_{op}^{apo}\}. \end{aligned} \quad (6)$$

Results

Two- and three-dimensional NMR studies were performed using both uniformly ^{15}N - and $^{15}\text{N}/^{13}\text{C}$ -labeled holoflavinodoxin. The corresponding gradient-enhanced $^1\text{H}-^{15}\text{N}$ HSQC spectrum of the 179-residue protein is shown in Figure 2 (for reasons of clarity, cross peaks are not numbered). The relatively large chemical shift dispersion observed is at least partly imposed by the presence of the FMN cofactor. Due to the relatively large size of the protein, however, several regions of cross peak overlap occur in the $^1\text{H}-^{15}\text{N}$ HSQC spectrum. These regions are marked by rectangles in Figure 2. In addition, the side-chain N-H₂ groups of the six Asn and the five Gln residues are identified, as are the indole N-H groups of the three Trp residues and the three cross peaks that are assigned to Arg side-chain N^ε-H groups. The N(3) atom of the FMN cofactor resonates at 159.3 ppm and its attached proton at 10.49 ppm. As a consequence of the spectral resolution required and the limitation of the total experiment time (Table 1), the N(3)H cross peak is folded in the ^{15}N dimension of the 2D $^1\text{H}-^{15}\text{N}$ HSQC experiment (Fig. 2) and in all 3D NMR experiments. The NMR measurements were done at pH 6.0 to minimize the rate of amide hydrogen exchange. Consequently, the number of amide hydrogens that are observed and that can be used to follow flavodoxin folding using hydrogen exchange pulse labeling methods is max-

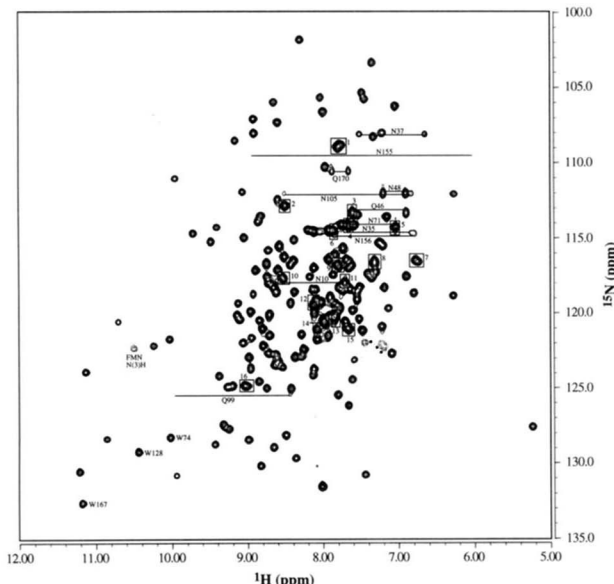


Fig. 2. Gradient-enhanced ^1H - ^{15}N HSQC spectrum of 5.2 mM ^{15}N -/ ^{13}C -labeled *A. vinelandii* holoflavodoxin II in 90% H_2O /10% $^2\text{H}_2\text{O}$ and 150 mM potassium pyrophosphate recorded at pH* 6.0, 303 K. Garp decoupling of ^{13}C was started shortly before transfer of magnetization to ^{15}N and lasted until the end of the acquisition period. Cross peaks of the indole N-H groups of the three Trp residues and of the N(3)H proton of the FMN cofactor are indicated. Horizontal lines connect the side-chain N-H₂ frequencies of the six Asn and the five Gln residues. The three cross peaks assigned to Arg side-chain N^c-H groups are indicated by *. Overlapping cross peaks are marked by rectangles. 1, Gly 12-Gly 97-Gly 176; 2, Ser 9-Thr 130; 3, Asp 68-Gln 46N^c; 4, Phe 117-Asn 71N^d; 5, Arg 24-Asn 71N^d; 6, Asp 32-Asn 35N^d-Gln 156N^c; 7, Tyr 47-Arg 120; 8, Leu 149-Gln 156; 9, Ser 20-Leu 78; 10, Asp 27-Ser 87; 11, Leu 177-Asn 10N^d; 12, Asp 85-Ala 109-Ala 165; 13, Asp 43-Ala 69; 14, Val 36-Phe 44-Ala 166; 15, Lys 2-Ala 122; 16, Phe 86-Lys 118. Folded cross peaks are represented by broken lines.

imized. Below pH 6.0, substantial precipitation of the protein occurred at concentrations suitable for NMR experiments.

Backbone assignments

The sequential assignment procedure started by picking cross peaks in the ^1H - ^{15}N HSQC spectrum to obtain the $^1\text{H}(i)$ and the $^{15}\text{N}(i)$ resonance frequencies. Due to overlap, less than the expected 173 non-prolyl backbone cross peaks were found. However, 172 backbone $^1\text{H}(i)$, $^{15}\text{N}(i)$, and $^{13}\text{CO}(i-1)$ correlations could be identified in the ct-HNCO spectrum, implying that the correlation for only one residue was missing. Using the combination of the CBCANH and the CBCA(CO)NH spectrum, first the $^{13}\text{C}^\alpha(i)$, $^{13}\text{C}^\alpha(i-1)$, $^{13}\text{C}^\beta(i)$, and $^{13}\text{C}^\beta(i-1)$ frequencies were determined. Note that, in some cases, overlap hampered this procedure. Second, both spectra were used to make sequential assignments to correlate residue(i) with its preceding residue($i-1$). In many cases, the $^{13}\text{C}^\alpha(i-1)$ and $^{13}\text{C}^\beta(i-1)$ resonances were not unique, resulting in a number of possible connecting residues. However, the sequential assignment for large stretches of the amino acid sequence was possible by making use of the characteristic $^{13}\text{C}^\alpha$ and/or $^{13}\text{C}^\beta$ chemical shifts of glycine, alanine, threonine, and serine residues in the CBCANH spectrum (Grzesiek & Bax, 1993). Figure 3 shows the sequential connectivities of residues

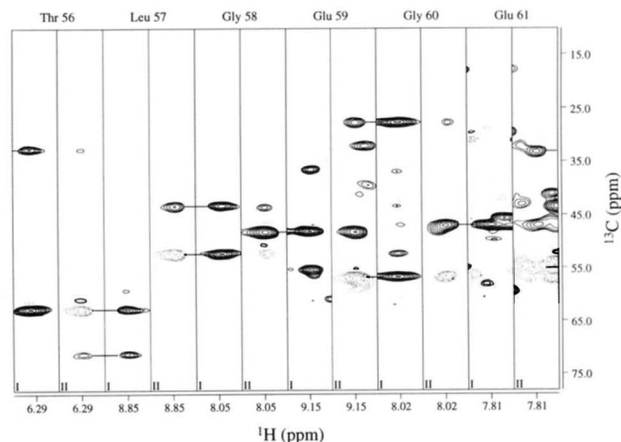


Fig. 3. ^1H - ^{15}N strips along the ^{13}C axes of the CBCA(CO)NH (I) and CBCANH (II) spectra of ^{15}N -/ ^{13}C -labeled *A. vinelandii* holoflavodoxin II in 90% H_2O /10% $^2\text{H}_2\text{O}$, pH* 6.0, 303 K. The sequential connectivities of Thr 56–Glu 61 are indicated by horizontal lines. Cross peaks with negative intensities are represented by broken lines.

Thr 56-Glu 61 in the ^1H - ^{15}N strips along the ^{13}C axes of the CBCA(CO)NH (I) and CBCANH (II) spectra. Due to the cancellation of the $^{13}\text{C}^\alpha$ and $^{13}\text{C}^\beta$ cross peak intensities of some Thr and Ser residues in the CBCANH spectrum, the HNCA spectrum was useful to ascertain the position of the $^{13}\text{C}^\alpha(i)$ frequencies. Inspection of the $^{13}\text{CO}(i-1)$ and $^{13}\text{CO}(i)$ correlations in the ct-HNCO and HN(CA)CO spectra resolved all previously existing ambiguities and resulted in the complete $^1\text{H}^\text{N}$, ^{15}N , $^{13}\text{C}^\alpha$, $^{13}\text{C}^\beta$, and ^{13}CO assignments. The ^{13}CO and $^{13}\text{C}^\alpha$ chemical shifts of the first residue, Ala 1, were determined using the ^1H - ^{15}N correlation of Lys 2. It appears that no $^1\text{H}^\text{N}$ and ^{15}N assignments can be found in any of the above-mentioned experiments for residue Gly 158, although its ^{13}CO and $^{13}\text{C}^\alpha$ chemical shifts could be determined using the ^1H - ^{15}N correlation of Lys 159. A recent NMR study of *Azotobacter chroococcum* flavodoxin shows that the amide proton of the equivalent Gly 159 residue is likewise not observed (Peelen et al., 1996).

The HBHA(CO)NH spectrum was used to assign the $^1\text{H}^\alpha$ resonances for all residues, except for those of the five residues preceding a proline and residues Ser 157 and Leu 179. The $^1\text{H}^\alpha$ resonance assignments were confirmed and completed using the HNHA spectrum. The $^1\text{H}^\alpha$ resonance of Ser 157 was present in the HNHA spectrum, albeit very weak, whereas the $^1\text{H}^\alpha$ resonance of Ala 172 was determined solely by relying on the ^{15}N -NOESY-HSQC and ^{15}N -TOCSY-HSQC/HMQC spectra. The HBHA(CO)NH spectrum, in combination with the HNHB, ^{15}N -NOESY-HSQC, and ^{15}N -TOCSY-HSQC/HMQC spectra, led to the assignment of the $^1\text{H}^\beta$ resonances. The $^1\text{H}^\alpha$ and $^1\text{H}^\beta$ resonance frequencies of residue Thr 130 appear to overlap. The only residue for which no $^1\text{H}^\beta$ assignment could be found is Leu 149. It is perhaps noteworthy that the $^1\text{H}^\alpha$ chemical shift of Leu 149 is 2.80 ppm; therefore, it is possible that the chemical shifts of the $^1\text{H}^\beta$ protons of Leu 149 overlap with that of its $^1\text{H}^\alpha$ proton. The side-chain N-H₂ groups of six Asn and five Gln residues and the indole N-H groups of the three Trp residues were assigned using the ^{15}N -NOESY-HSQC spectrum. The ^{15}N , $^1\text{H}^\alpha$, $^{13}\text{C}^\alpha$, $^1\text{H}^\alpha$, $^{13}\text{C}^\beta$, $^1\text{H}^\beta$, and ^{13}CO resonance assignments are listed in Table 1 of the supplementary material in the Electronic Appendix.

Table 1. Acquisition parameters for the various multidimensional NMR experiments

Experiment	Nucleus			No. of complex points			Spectral width (Hz)			Scans
	t_1	t_2	t_3	t_1	t_2	t_3	t_1	t_2	t_3	
^1H - ^{15}N -HSQC	^{15}N	^1H		384	512		1,863	8,065		32
ct-HNCO	^{13}C	^{15}N	^1H	110	42	512	2,153	2,235	9,615	12
CBCANH	^{13}C	^{15}N	^1H	52	32	512	8,547	1,863	8,065	32
CBCA(CO)NH	^{13}C	^{15}N	^1H	64	48	512	10,000	2,235	9,615	8
ct-HNCA	^{15}N	^{13}C	^1H	32	50	512	1,863	5,056	8,065	32
ct-HN(CA)CO	^{15}N	^{13}C	^1H	32	50	512	1,863	5,056	8,065	32
HBHA(CO)NH	^1H	^{15}N	^1H	64	48	512	4,316	2,235	9,615	16
ct-HNHA	^{15}N	^1H	^1H	48	44	512	1,863	4,651	8,065	32
HMQC-NOESY-HMQC	^{15}N	^{15}N	^1H	62	32	512	1,863	1,863	8,065	8
NOESY-HMQC	^1H	^{15}N	^1H	128	46	512	6,965	1,863	8,065	8
TOCSY-HSQC	^1H	^{15}N	^1H	64	32	512	6,965	2,235	9,615	8
TOCSY-HMQC	^1H	^{15}N	^1H	154	44	512	6,965	1,863	6,065	8
ct-HNHB	^{15}N	^1H	^1H	32	256	512	1,863	8,065	8,065	6

Secondary structure

The NMR data and the deduced secondary structure of holoflavinodoxin are summarized in Figure 4. Sequential and medium-range NOE connectivities are taken from a 50-ms ^{15}N -NOESY-HSQC and a 75-ms ^{15}N -HMQC-NOESY-HMQC spectrum. $^3J_{\text{HN}-\text{H}\alpha}$ coupling constants for 109 residues were determined using the HNHA spectrum. Only slowly exchanging amide protons [$\log(k_{ex}) < -5$, see below] are indicated in Figure 4. The consensus CSI as shown in Figure 4 was calculated using the chemical shift information of the $^1\text{H}^\alpha$, $^{13}\text{C}^\alpha$, ^{13}CO , and $^{13}\text{C}^\beta$ resonances (Wishart et al., 1992; Wishart & Sykes, 1994). Helical regions are identified by relatively strong $d_{\text{NN}(i,i+1)}$ contacts, relatively weak $d_{\alpha\text{N}(i,i+1)}$ contacts, the presence of $d_{\alpha\text{N}(i,i+3)}$ contacts, $^3J_{\text{HN}-\text{H}\alpha} < 6$ Hz, and a negative CSI, whereas β -strands are characterized by relatively weak $d_{\text{NN}(i,i+1)}$ contacts, relatively strong $d_{\alpha\text{N}(i,i+1)}$ contacts, $^3J_{\text{HN}-\text{H}\alpha} > 8$ Hz, and a positive CSI (Wüthrich, 1986; Wishart & Sykes, 1994). Furthermore, it is expected that stable secondary structure elements are characterized by relatively slow amide exchange behavior. As indicated in Figure 4, five β -strands and five α -helices are identified in holoflavinodoxin. The topology of the five-stranded parallel β -sheet ($\beta2-\beta1-\beta3-\beta4-\beta5$) expected for a flavodoxin was confirmed by the presence of long-range NOEs between backbone atoms (Fig. 5).

From the NOE contacts and hydrogen exchange data, we conclude that the hydrogen bonding network between strands $\beta 2$ and $\beta 1$ is irregular and that strand $\beta 2$ contains a two-residue β -bulge. As can be seen, strand $\beta 5$ is, in fact, composed of two parts, $\beta 5a$ and $\beta 5b$, which are separated by a 23-residue loop. The presence of this loop is characteristic of ‘long-chain’ flavodoxins. Although residues 133–139 in this 23-residue loop are characterized by a positive CSI, no long-range NOEs between the backbone atoms of these residues and backbone atoms in any strand of the parallel β -sheet are found, and the corresponding $^3J_{\text{HN}-\text{H}\alpha}$ values are smaller than 8 Hz for all but one residue. Similarly, no NOE contacts between backbone atoms of residues 38–40 and backbone atoms in the central parallel β -sheet could be identified, although these residues probably form a short extended structure because they are

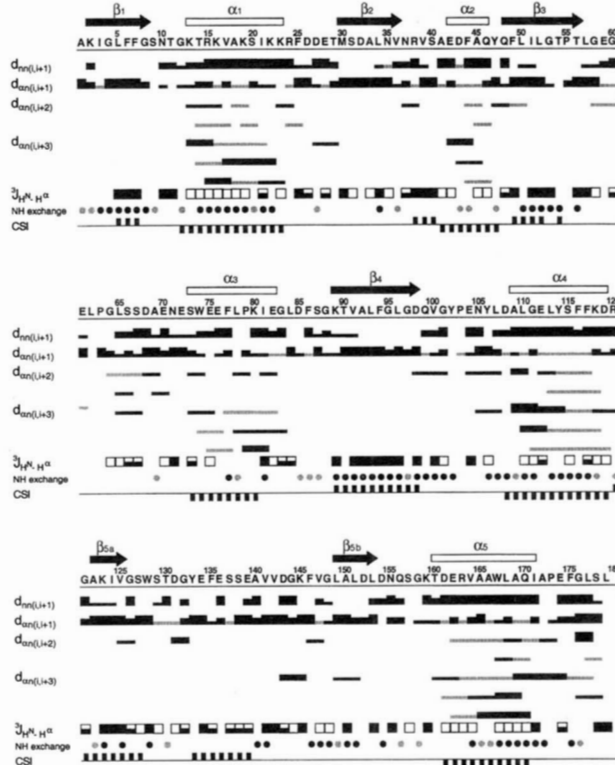


Fig. 4. Summary of NMR data obtained on *A. vinelandii* holoflavinodoxin II. Sequential and medium-range NOE connectivities are classified into strong, medium, and weak as indicated by the bar size. Small grey bars represent ambiguities due to spectral overlap. $^3J_{\text{HN}-\text{H}\alpha}$ coupling constants are classified as follows: < 6 Hz (□); $6-8$ Hz (■); > 8 Hz (■). Slowly exchanging amide protons [$\log(k_{ex}) < -5$] are marked by black dots. Grey dots represent amide protons for which the exchange rates could not be determined. The consensus CSI is positive for β -sheet and negative for α -helical conformations, respectively (Wishart et al., 1992; Wishart & Sykes, 1994). Deduced secondary structure elements are indicated above the amino acid sequence.

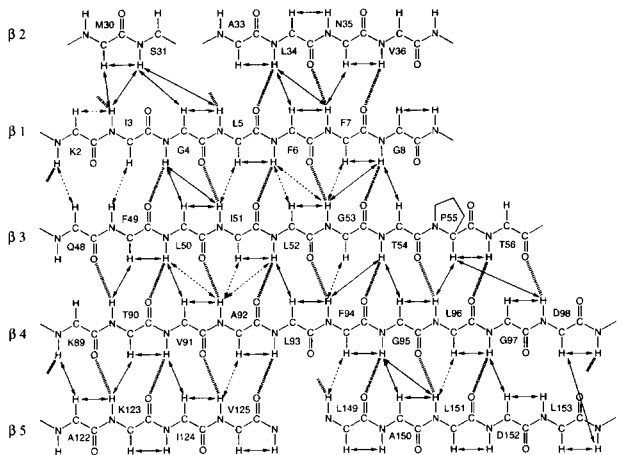


Fig. 5. Topology of the five-stranded β -sheet of *A. vinelandii* holoflavodoxin II. Solid arrows indicate unambiguous NOE contacts; dashed arrows represent NOE contacts that are ambiguous due to spectral overlap. Weak $d_{\alpha N(i,i+1)}$ contacts are not shown. Hydrogen bonds as expected from slow amide proton exchange and NOE contacts are indicated by |||||. Exchange of the amide protons of Lys 2, Val 36, and Leu 149 indicated to be slow is uncertain due to spectral overlap.

characterized by strong $d_{\alpha N(i,i+1)}$ contacts, a positive CSI, and large $^3J_{HN-H\alpha}$ values. Strands $\beta 2$ and $\beta 5b$ were not identified via the CSI, although the $\Delta^{13}\text{CO}$ chemical shifts did identify these regions as being β -sheet. From Figure 4, we can conclude that the prediction of secondary structure elements in holoflavodoxin by the CSI was more successful for the five α -helical regions than for the regions comprising β -strands. Our results seem to support the observation that α -helices are better defined by the $\Delta^{13}\text{C}^\alpha$ chemical shift than β -strands (Remerowski et al., 1994).

FMN binding and tertiary contacts

Besides the general topology, some features of the tertiary structure of holoflavodoxin could relatively easily be identified using the NOE contacts of the N(3)H proton of the FMN cofactor and the NOE contacts of the indole N-H protons of the three tryptophan residues.

NOEs were observed between the N(3)H proton of the FMN cofactor and the amide protons of both Leu 107 and Asp 108, the $^1\text{H}^\alpha$ proton of Tyr 106, the $^1\text{H}^\beta$ atom of Thr 56, a $^1\text{H}^\beta$ atom of both Tyr 102 and Asn 105, and the methyl group of Thr 56. These NOEs define the FMN binding site around the N(3)H proton of FMN.

The NOE contacts of the indole proton of Trp 74 with the amide proton of Gly 8, the $^1\text{H}^\alpha$ proton of Phe 7, and both the $^1\text{H}^\alpha$ and $^1\text{H}^\beta$ proton of Thr 54 show that helix $\alpha 3$ is situated close to the C-terminal end of strands $\beta 1$ and $\beta 3$.

The NOE contacts of the indole N-H atoms of the remaining two tryptophan residues in combination with a careful inspection of the NOE contacts of the backbone atoms of residues 126–148 revealed several features of the 23-residue loop. First, an NOE between the amide protons of Trp 128 and Phe 146 shows that these atoms are in close proximity to each other. Second, the amide protons of residues 133–138 are all in close proximity of a side-chain ring proton of Trp 128, which explains the positive CSI observed for these residues. Third, several long-range NOE contacts anchor the

loop to the rest of the molecule. The indole proton of Trp 128 shows an NOE to the amide proton of Ala 150, a residue situated in strand $\beta 5b$, whereas the indole proton of Trp 167, a residue situated in helix $\alpha 5$, shows NOE contacts to the $^1\text{H}^\alpha$ protons of Gly 126 as well as to the amide proton of Leu 149, the first residue of strand $\beta 5b$. Fourth, several intraloop NOEs are found. As deduced from the NOE interactions between residues Val 141, Val 142, Lys 145, Phe 146, and Val 147, residues 140–147 are involved in a short antiparallel β -sheet structure. The latter is supported by the large $^3J_{HN-H\alpha}$ values of residues 141, 142, and 145 and the slow amide exchange behavior of residues 140, 141, 146, and 147 (Fig. 4). In addition, no significant differences between cross peak linewidths of backbone atoms of the loop residues and those of the remainder of the molecule were observed. All results support the conclusion that the 23-residue loop is structurally well defined and packed onto the remainder of the molecule.

Hydrogen exchange kinetics and apparent local stability

The exchange rates for the individual amide protons were extracted from the time dependence of their corresponding cross peak intensities in a series of $^1\text{H}-^{15}\text{N}$ HSQC spectra acquired after transfer of the lyophilized protein into $^2\text{H}_2\text{O}$ (150 mM potassium pyrophosphate, pH* 6.2 and 303 K). The $^1\text{H}-^{15}\text{N}$ HSQC spectra of 4.3 mM uniformly ^{15}N -labeled holoflavodoxin were recorded over a 42-h period. Both the first and the last $^1\text{H}-^{15}\text{N}$ HSQC spectrum recorded are shown in Figure 6. Thirty-six amide protons of holoflavodoxin exchanged so rapidly in $^2\text{H}_2\text{O}$ that no exchange rate could be determined ($k_{ex} \geq 10^{-2} \text{ s}^{-1}$). In contrast, 54 amide protons did not show any decrease in cross peak intensity over 42 h ($k_{ex} \leq 10^{-7} \text{ s}^{-1}$), as can be inferred from Figure 6. For 57 amide protons, the time dependence of their corresponding cross peak intensities could be fitted to a single exponential decay function (Equation 9) and individual exchange rates were determined. As an example, the decrease in cross peak intensity with time of the N(3)H proton of the functionally important FMN cofactor is shown in Figure 7. The N(3)H proton exchanged slowly, $k_{ex} = 7.3 \times 10^{-6} \text{ s}^{-1}$. Due to spectral overlap, the exchange rates of 25 backbone amide protons were not determined. Of the side-chain N-H protons, the cross peak intensities of the indole protons of Trp 74 and Trp 167 did not decrease in 42 h, whereas the indole proton of Trp 128 exchanged slowly ($k_{ex} = 2.0 \times 10^{-5} \text{ s}^{-1}$). Other side-chain N-H protons were already exchanged in the first $^1\text{H}-^{15}\text{N}$ HSQC spectrum recorded after initiation of exchange.

The logarithm of the exchange rate as a function of residue number is shown in Figure 8A. Using Equation 6, the ΔG_{op}^{app} value for each residue (Fig. 8B) was calculated; values vary from 2.7 kcal·mol $^{-1}$ to 8.7 kcal·mol $^{-1}$. The ΔG_{op}^{app} value for the amide protons that exchanged too fast to be observed in the first $^1\text{H}-^{15}\text{N}$ HSQC spectrum was set to 1.36 kcal·mol $^{-1}$, whereas the ΔG_{op}^{app} value for amide protons that had not exchanged in 42 h was estimated to be $\geq 9.54 \text{ kcal} \cdot \text{mol}^{-1}$. The $\log(k_{ex})$ and ΔG_{op}^{app} values for all residues are given in Table 2 of the supplementary material in the Electronic Appendix.

In general, the most stable regions of holoflavodoxin coincide with the identified secondary structure elements, whereas the less stable regions are the loop and turn elements. This is illustrated in Figure 9, which shows the X-ray structure of the highly homologous *A. chroococcum* flavodoxin (Thorneley et al., 1994) color-coded according to the exchange behavior of the corresponding amide protons in *A. vinelandii* holoflavodoxin II. Bearing in mind

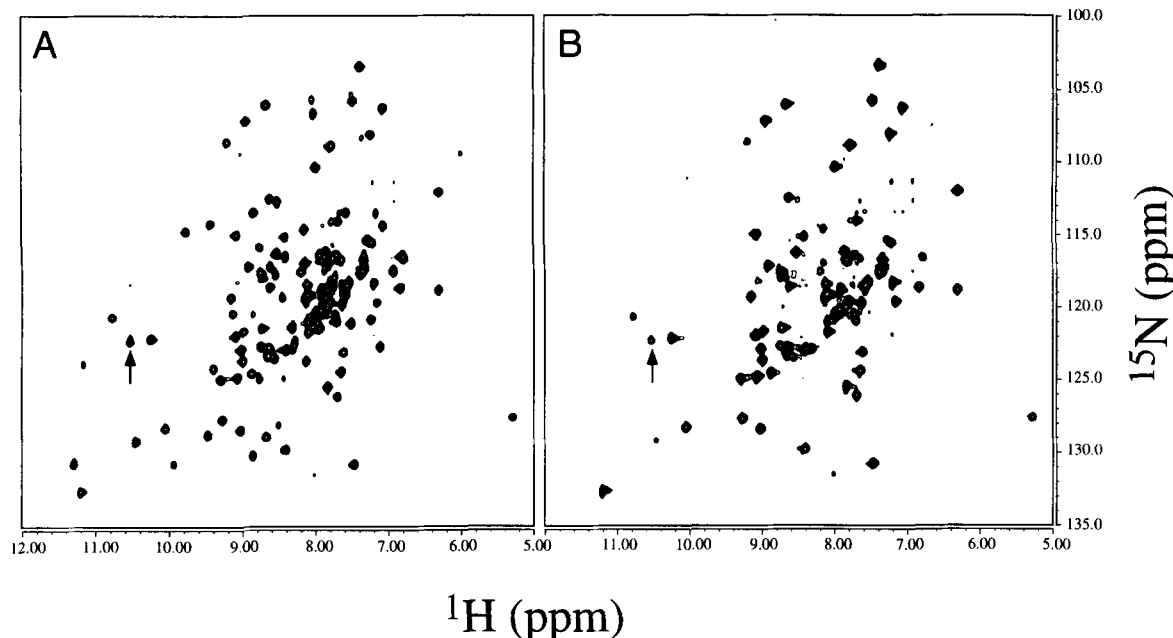


Fig. 6. Gradient-enhanced ^1H - ^{15}N HSQC spectra of 4.3 mM ^{15}N -labeled *A. vinelandii* holoflavinodoxin II (in 150 mM potassium pyrophosphate, pH* 6.2, 303 K) acquired (A) 10 min and (B) 42 h after transfer of the lyophilized protein into 99.9% $^2\text{H}_2\text{O}$. The folded N(3)H cross peak of the FMN cofactor is indicated by an arrow in both spectra.

that the first three N-terminal amide protons in an α -helix are generally not hydrogen bonded, we can conclude from Figures 8 and 9 that helices $\alpha 2$ and $\alpha 3$ are structurally less stable than the other α -helices of holoflavinodoxin. Not surprisingly, the two outer strands of the β -sheet, $\beta 2$ and $\beta 5$, are less stable than the three inner strands, because only half of the amide protons of the outer strands are involved in hydrogen bonds within the β -sheet (Fig. 5).

As discussed, the 23-residue loop intersecting strand $\beta 5$ (residues 126–148) is structurally well defined and packed onto the

remainder of the molecule. This loop is also relatively stable because the amide protons of Trp 128, Ala 140, Val 141, Phe 146, Val 147, and Gly 148 exchange with $k_{ex} < 10^{-5} \text{ s}^{-1}$ and because the majority of the remaining amide protons show intermediate exchange. In holoflavinodoxin, most loops connecting an α -helix to a β -strand or vice versa consist of six or less residues. These short loops are all characterized by fast amide exchange. The loops connecting strand $\beta 3$ with helix $\alpha 3$ (residues 57–72, 60's loop) and strand $\beta 4$ with helix $\alpha 4$ (residues 99–108, 100's loop) are rela-

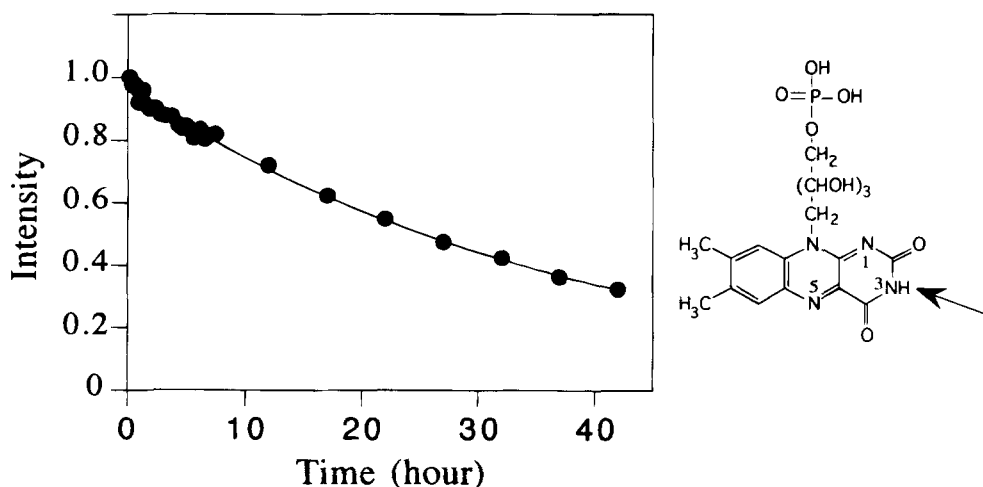


Fig. 7. Time-dependent decrease in ^{15}N - ^1H cross peak intensity of the N(3)H proton of the FMN cofactor (indicated by an arrow) after transfer of *A. vinelandii* holoflavinodoxin II into 99.9% $^2\text{H}_2\text{O}$. Intensities were normalized to the intensity of the first data point. The solid line is a least-squares fit of the data to a single exponentially decaying function with $k_{ex} = 7.3 \times 10^{-6} \text{ s}^{-1}$.

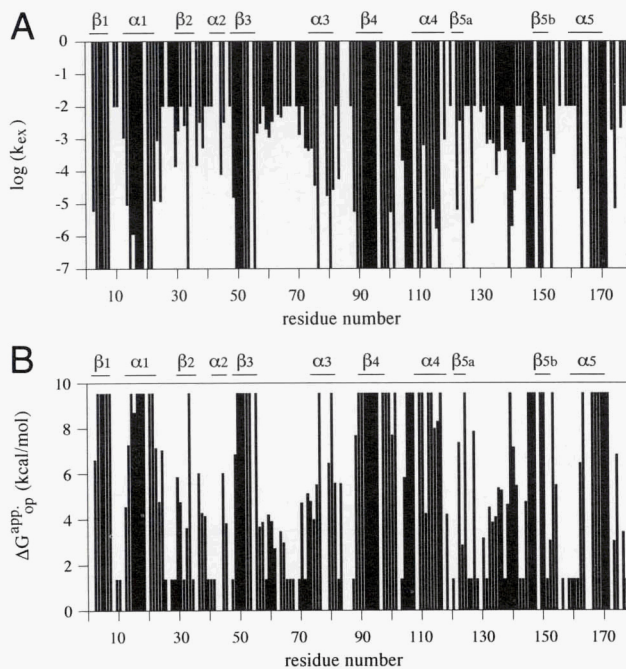


Fig. 8. Logarithm of (A) the amide proton exchange rate and (B) the calculated apparent free energy ΔG_{app} (298 K) versus residue number in *A. vinelandii* holoflavoxin II. For amide protons that exchanged so rapidly that they were not observed in our experiments in $^2\text{H}_2\text{O}$ (150 mM pyrophosphate, pH* 6.2, 303 K), $\log(k_{ex})$ was set to -2.00 (and ΔG_{app} to 1.36 kcal·mol⁻¹). For amide protons that had not exchanged in 42 h, $\log(k_{ex})$ was set to -7.00 (and ΔG_{app} to 9.54 kcal·mol⁻¹). Due to spectral overlap, the exchange rates of 25 backbone amide protons could not be determined.

tively long (Fig. 9). Whereas all amide protons in the 60's loop exchange rapidly, interestingly, most of the amide protons in the 100's loop do not exchange in 42 h.

Discussion

Structure of holoflavoxin and FMN binding site characteristics

The NMR results presented here (Figs. 4, 5) delineate the α/β doubly wound topology (Fig. 1) for *A. vinelandii* holoflavoxin II: a central five-stranded parallel β -sheet ($\beta_2\text{-}\beta_1\text{-}\beta_3\text{-}\beta_4\text{-}\beta_5$) that is surrounded by five α -helices. Note that helix $\alpha 2$ has not always been identified in flavodoxin structures, because it mostly occurs as a short nonregular α -helix or as a 3_{10} -helix. The two outer strands $\beta 2$ and $\beta 5$ of the five-stranded β -sheet are irregular. Strand $\beta 2$ contains a two-residue β -bulge that has so far only been identified in the flavodoxins of *Chondrus crispus* (Fukuyama et al., 1992) and of *A. chroococcum* (Peelen et al., 1996). Strand $\beta 5$ is interrupted by a 23-residue loop characteristic of long-chain flavodoxins; nonetheless, the hydrogen bonding pattern between strands $\beta 4$ and $\beta 5$ does not seem to be interrupted.

Many interactions exist between the noncovalently bound FMN cofactor and the apoprotein. The nucleotide phosphate binding motif S/T-X-T-G-X-T, which is conserved in the entire flavodoxin family, is located at the end of strand $\beta 1$ and the beginning of helix $\alpha 1$. The measured $^3J_{\text{HN-H}\alpha}$ values for residues Asn 10 (10.7 Hz), Thr 11 (10.7 Hz), Lys 13 (5.8 Hz), and Thr 14 (3.8 Hz) are in



Fig. 9. RasMol drawing (Sayle & Milner-White, 1995) of the X-ray structure of *A. chroococcum* flavodoxin (Thorneley et al., 1994). The structure is colored according to the exchange behavior of the corresponding backbone amide protons in the highly homologous *A. vinelandii* holoflavoxin II (pH* 6.2, 303 K). Red indicates amide protons that exchanged so rapidly that they were not observed in our experiments in $^2\text{H}_2\text{O}$ [$\log(k_{ex}) \geq -2$]; green indicates amide protons with $-5 < \log(k_{ex}) < -2$; blue indicates amide protons that had not exchanged after 42 h in 99.9% $^2\text{H}_2\text{O}$ or that exchanged very slowly [$\log(k_{ex}) \leq -5$]; yellow indicates that the exchange rate could not be determined for a residue. Note that the N(3)H proton of the FMN cofactor exchanges very slowly, $\log(k_{ex}) = -5.14$. However, for reasons of clarity, the cofactor is depicted in black.

accordance with the typical ϕ/ψ values found for residues forming this loop conformation (Swindells, 1993) (unfortunately, the $^3J_{\text{HN-H}\alpha}$ value for residue Gly 12 could not be determined due to spectral overlap). As can be deduced from the extreme downfield shifts of the amide protons of Asn 10, Thr 11, Lys 13, and Thr 14 in *A. vinelandii* holoflavoxin II, these amide protons are involved in a hydrogen bonding network with the phosphate group of the FMN cofactor. However, the rapid amide proton exchange behavior of residues 10, 11, and 13 indicates that the phosphate binding site in holoflavoxin is locally not very stable.

The isoalloxazine ring of the FMN cofactor is in contact with two different regions of the apoprotein that form the FMN binding site: (1) residues situated at the end of strand $\beta 3$ (here: among others Thr 56) and (2) residues in the loop between strand $\beta 4$ and helix $\alpha 4$ (here: among others Tyr 102–Asp 108, 100's loop). In most flavodoxins, the isoalloxazine ring is bracketed by two aromatic side chains (Grandori & Carey, 1994): a tryptophan ring is located at the side of the ribityl side chain of the FMN, and a tyrosine ring is nearly coplanarly stacked at the other side of the isoalloxazine ring.

Interestingly, the “conserved” tryptophan residue is replaced by a leucine residue (Leu 57, *A. vinelandii* flavodoxin numbering) in flavodoxins from *Azotobacter*, *Klebsiella pneumoniae*, and *Enterobacter agglomerans*. Apparently, the presence of an aromatic ring

at this position is not a prerequisite to acquire a low E_1 redox potential, because the E_1 redox potentials of *Azotobacter* flavodoxins are among the lowest in the flavodoxin family. Concomitantly, the loop between strand $\beta 3$ and helix $\alpha 3$ is inserted by a few extra residues (roughly residues 65–70, 60's loop). Recently, Peelen et al. (1996) found that residues Ser 67 and Asn 71 (*A. vinelandii* flavodoxin numbering) in the 60's loop in *A. chroococcum* flavodoxin are involved in the interaction with the Fe protein of the vanadium nitrogenase complex. The fast amide exchange behavior of residues in the 60's loop observed by us implies that all amide protons are solvent accessible and/or locally unfold.

Tyr 102 in the 100's loop of *A. vinelandii* flavodoxin II is conserved within a large part of the flavodoxin family. We observe an NOE contact between the N(3)H proton of FMN and a $^1\text{H}^\beta$ atom of Tyr 102. The N(3)H proton also shows NOE connectivities to residues Asn 105, Tyr 106, Leu 107, and Asp 108 in the 100's loop. The amide protons of most residues in this loop did not exchange in 42 h in 99.9% $^2\text{H}_2\text{O}$ and the N(3)H proton exchanges rather slowly ($k_{ex} = 7.3 \times 10^{-6} \text{ s}^{-1}$). This implies that the 100's loop surrounding the pyrimidine part of the FMN molecule forms a structurally stable unit. From a comparison with known flavodoxin structures and sequences, we infer that the N(3)H proton of FMN forms a hydrogen bond with the carbonyl oxygen of Asn 105.

Apparent local stability of the secondary structure of holoflavodoxin

The most stable and regular α -helices in holoflavodoxin are helices $\alpha 1$ and $\alpha 5$, which face the same side of the hydrophobic central parallel β -sheet (Figs. 4, 8, 9), although some dispute about the beginning and the end of the α -helices is possible. Most likely, the regular helix $\alpha 5$ ends before Pro 173, whereas the remainder of the C-terminal residues form an additional 3_{10} -helical structure. Helix $\alpha 2$ has been characterized by $d_{an(i,i+3)}$ contacts, small $^3J_{\text{HN-H}\alpha}$ values, and a negative CSI (Fig. 4). However, the fast amide proton exchange behavior shows that the local stability of this secondary structure element is rather low. Similarly, helix $\alpha 3$ is not very stable structurally because it is characterized by only two slowly exchanging amide protons. Furthermore, the unusually high $^3J_{\text{HN-H}\alpha}$ value of Ile 81 points to an irregularity in this α -helix. The fast exchange of the amide proton of Glu 112 in helix $\alpha 4$ and the intermediate $^3J_{\text{HN-H}\alpha}$ value of this residue and of Phe 117 indicate that helix $\alpha 4$ is not completely regular either.

The central five-stranded parallel β -sheet consists mainly of hydrophobic residues and forms the stable core of the protein. The amide protons of almost all of these residues, which are involved in the hydrogen bonding network, do not show any exchange after 42 h in 99.9% $^2\text{H}_2\text{O}$. The apparent local stability, ΔG_{op}^{app} , of residues in the flavodoxin core is $\geq -9.5 \text{ kcal} \cdot \text{mol}^{-1}$. Exchange of the most protected amide protons in proteins has been shown to occur often via global unfolding (Wagner & Wüthrich, 1979; Woodward, 1994; Jeng & Dyson, 1995; Englander et al., 1996). We propose that kinetic and equilibrium global unfolding of holoflavodoxin only occurs after release of the FMN cofactor. This means that exchange of amide protons within the core of the protein with the solvent is only possible from the apo state of the protein. Consequently, K_{op}^{holo} (Equation 6) will equal zero for these amide protons and Equation 6 can be rewritten to

$$\Delta G_{op}^{app} = -RT \ln f_{apo} * K_{op}^{apo} = -RT \ln \{K_d / [\text{FMN}]\} + \Delta G_{op}^{apo}. \quad (7)$$

Using the known dissociation constant for flavin release of *A. vinelandii* flavodoxin (Pueyo et al., 1996), ΔG_{op}^{apo} is determined to be $> -4.7 \text{ kcal} \cdot \text{mol}^{-1}$. This agrees with the free energy of global unfolding of *A. vinelandii* apoflavodoxin II, ΔG_{unf} of $5.6 \pm 0.6 \text{ kcal} \cdot \text{mol}^{-1}$, which is determined via guanidinium hydrochloride-induced equilibrium denaturation of apoflavodoxin using both fluorescence and CD spectroscopy (C.P.M. van Mierlo, unpubl. results). For amide protons in holoflavodoxin not belonging to the stable core of the protein, it is not possible at this point to distinguish whether the measured amide proton exchange takes place in the holo- and/or the apoprotein.

Analogous to the amide proton exchange behavior (Equation 5), hydrogen exchange of the N(3)H proton of the FMN cofactor can occur in two distinct situations: (1) when the FMN cofactor is free in solution, and/or (2) when it is bound to the apoprotein and local unfolding movements make the N(3)H amenable to hydrogen exchange:

$$\begin{aligned} k_{ex}^{\text{N}(3)\text{H}} &= f_{\text{FMN}} * k_{int}^{\text{N}(3)\text{H}} + f_{\text{holo}} * k_{ex}^{\text{holo}}, \\ &= f_{\text{FMN}} * k_{int}^{\text{N}(3)\text{H}} + f_{\text{holo}} * K_{op}^{\text{holo}} * k_{int}^{\text{N}(3)\text{H}}, \end{aligned} \quad (8)$$

with f_{FMN} , the fraction free FMN in solution and $k_{int}^{\text{N}(3)\text{H}}$, the intrinsic exchange rate of the N(3)H proton in free FMN. If we assume that the N(3)H proton of FMN only exchanges with the solvent when the cofactor is free in solution, $k_{int}^{\text{N}(3)\text{H}}$ is calculated to be 0.02 s^{-1} . Because exchange can, in principle, occur in both situation 1 and situation 2, this calculated value of 0.02 s^{-1} represents the upper limit for $k_{int}^{\text{N}(3)\text{H}}$. For comparison, calculated values of k_{int} for amide protons vary roughly between 0.3 s^{-1} and 17 s^{-1} under our experimental conditions. The fact that amide protons of many residues in the 100's loop surrounding N(3)H exchange significantly slower than the N(3)H proton of the FMN cofactor itself, although their k_{int} values are equivalent or larger than $k_{int}^{\text{N}(3)\text{H}}$, suggests that (1) the observed N(3)H proton exchange takes mainly place while FMN is free in solution (situation 1) and that (2) many amide protons of residues in the 100's loop are to a large extent protected against hydrogen exchange in the apoprotein.

Implications for redox potential regulation

Both the E_1 and the E_2 redox potential of flavodoxins are regulated by specific interactions between the FMN cofactor and apoflavodoxin. A few factors are known to influence the E_1 redox potential. For example, a single negative charge from either an acidic side-chain group or from the 5'-phosphate group of the FMN cofactor, both within 13 Å of the N1 atom of FMN, contributes -15 mV to the E_1 redox potential in *Desulfovibrio vulgaris* flavodoxin (Zhou & Swenson, 1995, 1996a), whereas the unfavorable coplanar stacking of the conserved tyrosine side chain with the flavin ring contributes -140 mV to the E_1 redox potential in this protein (Stockman et al., 1994; Swenson & Krey, 1994; Zhou & Swenson, 1996b). Furthermore, it is thought that a nonpolar environment of the two-electron reduced hydroquinone anion destabilizes this oxidation state (van Mierlo et al., 1990a; Zhou & Swenson, 1996b).

Our finding that the N(3)H proton probably does not exchange when the cofactor is bound to apoflavodoxin indicates that this region of the FMN binding site is highly solvent inaccessible. The solvent inaccessibility of the nonpolar environment around N(3)

could at least in part establish the low E_1 redox potential of *A. vinelandii* holoflavinodoxin II ($E_{1,\text{pH}8.5} = -485$ mV; Steensma et al., 1996). A comparison of the N(3)H proton exchange behavior in the oxidized state and the E_1 redox potential of flavodoxins from other organisms shows, as yet, no simple and straight-forward relation. The hydrogen exchange behavior of the N(3)H proton of the FMN cofactor is reported to be slow in *Anabaena* 7120 flavodoxin (Stockman et al., 1988), moderate in *Anacystis nidulans* flavodoxin (Clubb et al., 1991), and fast in *D. vulgaris* flavodoxin (Stockman et al., 1993), whereas their $E_{1,\text{pH}7}$ redox potentials are -425 mV, -447 mV, and -438 mV, respectively. This illustrates that most likely a different interplay of various interactions between the FMN cofactor and apoflavodoxin optimizes the functional E_1 redox potential in each flavodoxin species.

The function of the 23-residue insertion in strand $\beta 5$ in long-chain flavodoxins is unclear and certainly no distinction between long-chain and short-chain flavodoxins can be made on the basis of their respective E_1 redox potentials. We propose that the presence of the 23-residue loop enhances the structural stability of *A. vinelandii* holoflavinodoxin II, because it specifically enables the 100's loop to form a rigid and stable hydrogen bonding network with the FMN cofactor. In the semiquinone state, this could result in an enhanced binding and thus a more negative E_1 redox potential, or alternatively, an enhanced structural stability of holoflavinodoxin in the two-electron reduced state might be necessary to keep the reduced FMN cofactor bound. This can also explain our results that removal of the 23-residue loop in *A. vinelandii* flavodoxin II by site-directed mutagenesis does not lead to any detectable flavodoxin accumulation in *Escherichia coli* cells.

Implications for flavodoxin folding

The chemotactic protein Che Y shares the α/β doubly wound topology with the flavodoxin family, although little or no significant sequence homology can be detected between these proteins (Bowie et al., 1990). The structure of the transition state for unfolding of Che Y, as determined via mutational studies and Φ -value analysis (López-Hernández & Serrano, 1996; López-Hernández et al., 1997), can be divided into a partly folded subdomain 1 (comprising the first half of the protein: $\beta 1$, $\alpha 1$, $\beta 2$, $\alpha 2$, and $\beta 3$) and a disorganized subdomain 2 (comprising the second half of the protein: $\beta 3$, $\alpha 3$, $\beta 4$, $\alpha 4$, $\beta 5$, and $\alpha 5$) (see Fig. 1). Hydrogen exchange measurements on Che Y indicate that amide protons in subdomain 1 are generally more protected against exchange and that subdomain 2 is characterized by a rather poor overall stability and increased flexibility (Bruix et al., 1997). Our results on an α/β doubly wound protein do not support the latter observation. We do not find any evidence that *A. vinelandii* holoflavinodoxin II is divided into two subdomains based on its amide proton exchange rates (see Figs. 8 and 9). A study of the kinetic folding pathway of *A. vinelandii* holo- and apoflavodoxin II will conclusively reveal whether flavodoxin folding is also initiated by the nucleation and condensation of subdomain 1, as has been proposed for the structurally homologous protein Che Y (López-Hernández & Serrano, 1996; Bruix et al., 1997).

Conclusion

In this study, the ^{15}N , $^1\text{H}^N$, $^{13}\text{C}^\alpha$, $^1\text{H}^\alpha$, $^{13}\text{C}^\beta$, $^1\text{H}^\beta$, and ^{13}CO resonance assignments of *A. vinelandii* holoflavinodoxin II are presented. Furthermore, the determination of the solution secondary

structure of holoflavinodoxin has established the expected α/β doubly wound topology and unraveled its FMN binding characteristics.

Our results of the hydrogen exchange experiment indicate that the amide protons of 65 residues and three indole side-chain protons exchange relatively slowly ($k_{ex} < 10^{-5}$ s $^{-1}$). This ensures that it is feasible to perform pulsed hydrogen exchange experiments to study the folding pathway of flavodoxin by NMR spectroscopy. Because the slowly exchanging amide protons are located in all regular secondary structure elements (with the exception of helix $\alpha 2$), as well as in the 23-residue loop intersecting strand $\beta 5$ and in the 100's loop surrounding the N(3)H proton of the FMN cofactor, it should be possible to study the kinetic folding process of *A. vinelandii* holoflavinodoxin II in great structural detail.

Materials and methods

Materials

Recombinant *A. vinelandii* (strain ATCC 478) C69A holoflavinodoxin II was expressed in *E. coli* TG2 (unpubl. results). Uniformly ^{15}N -labeled protein was produced by growing bacteria for 40 h at 37 °C on minimal medium containing 0.5 g/L $^{15}\text{NH}_4\text{Cl}$ (Campro Scientific, Veenendaal, Netherlands), 6 g/L Na_2HPO_4 , 3 g/L KH_2PO_4 , 0.5 g/L NaCl , 2 mM MgSO_4 , 0.1 mM CaCl_2 , 10 μM FeCl_3 , 5 mg/L thiamine, 3 g/L glucose, 50 mg/L Amp, and 20 mg/L IPTG.

$^{15}\text{N}/^{13}\text{C}$ -labeled protein was produced by growing *E. coli* TG2 for 30 h at 37 °C on medium containing 2 g/L uniformly ^{13}C -labeled sugars and 1 g/L uniformly $^{13}\text{C}/^{15}\text{N}$ -labeled pepton (EMBL-mix, J. Ashurst & H. Oschkinat, EMBL, Germany), 8 g/L Na_2HPO_4 , 2 g/L KH_2PO_4 , 0.5 g/L NaCl , 0.3 mM Na_2SO_4 , 1 mM MgSO_4 , 0.3 mM CaCl_2 , 5 mg/L thiamine, *E. coli* trace elements (EDTA, FeCl_3 , ZnCl_2 , CuCl_2 , $\text{CoCl}_2 \cdot 6\text{H}_2\text{O}$, H_3BO_3 , $\text{MnCl}_2 \cdot \text{H}_2\text{O}$), 50 mg/L Amp, and 20 mg/L IPTG.

Purification and sample preparation

Holoflavinodoxin was purified as described by Tollin and Edmondson (1980). Uniformly ^{15}N -labeled holoflavinodoxin was transferred to a potassium pyrophosphate buffer via gel filtration. After subsequent lyophilization, the protein was dissolved in 500 μL 90% $\text{H}_2\text{O}/10\%$ $^{2}\text{H}_2\text{O}$ to yield a 3.5 mM protein solution in 150 mM potassium pyrophosphate, pH* 6.0. Uniformly $^{15}\text{N}/^{13}\text{C}$ -labeled holoflavinodoxin was transferred to a potassium pyrophosphate buffer via gel filtration and subsequently concentrated via ultra-filtration using a Filtronmicrosep centrifugal concentrator. The final 500- μL sample contained 5.2 mM protein in 150 mM potassium pyrophosphate in 90% $\text{H}_2\text{O}/10\%$ $^{2}\text{H}_2\text{O}$, pH* 6.0. TSP was always present in minute amounts as an internal standard and all samples were successively evacuated and filled with argon at least four times.

NMR spectroscopy

General

All experiments were recorded at 303 K on a Bruker AMX 500 or a Bruker AMX2600 spectrometer equipped with either a triple-resonance 5-mm inverse probe or a triple-resonance 5-mm inverse probe with a self-shielded z -gradient. Presaturation of the water signal was employed during the 1.25-s relaxation delay period for the non-gradient-enhanced NMR experiments. No presaturation

was used during the relaxation delay period in the gradient-enhanced experiments.

^{15}N decoupling during acquisition was accomplished using the GARP sequence with a 1.4-kHz rf field strength (Shaka et al., 1985). On the Bruker AMX 500 spectrometer, off-resonance excitation of the ^{13}C nucleus was accomplished by the application of phase-modulated pulses with an amplitude profile corresponding to the center lobe of a sinc function (Patt, 1992). Unless stated otherwise, standard de- and rephasing delays were used in the heteronuclear pulse sequences. The ^1H carrier frequency was positioned at the water resonance during the experiments, unless stated otherwise. The ^{15}N carrier position was at 118 ppm. Depending on the experiment, the ^{13}C carrier was placed in the middle of the C^α region (at 77 ppm), in the middle of the CO region (at 183 ppm), or in the middle of the $\text{C}^\alpha/\text{C}^\beta$ region (at 45 ppm).

Quadrature detection in all indirect dimensions was accomplished using the States-TPPI method (Marion et al., 1989b) for the nongradient-enhanced experiments, whereas for the gradient-enhanced experiments, this was obtained by alternate N-and P-type selection (Kay et al., 1992) for each sensitivity-enhanced indirect dimension (Cavanagh & Rance, 1990; Palmer et al., 1991; Wijmenga et al., 1996). Pulsed field gradients have a sine-bell shape, with a duration of either 1 ms or 0.5 ms and gradients strengths are set to 80 and 16, respectively, where a gradient strength of 100 corresponds to ca. 60 G/cm at the center of the gradient.

Multidimensional NMR experiments

^1H - ^{15}N correlations were obtained using a gradient-enhanced ^1H - ^{15}N HSQC (Palmer et al., 1991; Kay et al., 1992) experiment, which employs a selective Gaussian water flip-back pulse (Stonehouse et al., 1994), and a ct-HNCO (Grzesiek & Bax, 1992a; Jahnke & Kessler, 1994) experiment. Sequential assignments were made using a CBCANH (Grzesiek & Bax, 1992b) experiment in combination with a gradient-enhanced CBCA(CO)NH (Grzesiek & Bax, 1992c; Peelen et al., 1996) experiment, and a ct-HNCO experiment in combination with a ct-HN(CA)CO (Clubb et al., 1992) experiment, respectively. The ct-HN(CA)CO experiment was modified to include a DIPSI-2 proton decoupling sequence (Shaka et al., 1988) between the refocused INEPT and the refocused reverse INEPT transfer periods. To complete the assignments of all backbone atoms, a ct-HNCA (Grzesiek & Bax, 1992a) experiment and a gradient-enhanced HBHA(CO)NH experiment (Grzesiek & Bax, 1992c, 1993; Peelen et al., 1996) were acquired. In the indirect ^1H dimension of the HBHA(CO)NH experiment, the carrier was positioned in the middle of the amide region. A 3D gradient-enhanced HNHB (Archer et al., 1991) experiment was recorded to unequivocally assign some $^1\text{H}^\beta$ resonances.

Three-dimensional ^{15}N -separated NOESY-HMQC (Marion et al., 1989a) and HMQC-NOESY-HMQC (Frenkiel et al., 1990; Ikura et al., 1990) spectra were acquired using mixing times of 50 ms and 75 ms, respectively. In the NOESY-HMQC and the HMQC-NOESY-HMQC experiment, no gradients were applied and, hence, the water signal was saturated during both the mixing period and the relaxation delay period. A 3D ^{15}N -separated TOCSY-HMQC (Marion et al., 1989a) experiment was acquired using a 25.8-ms clean-DIPSI-2 mixing sequence (Cavanagh & Rance, 1992). Furthermore, a doubly sensitivity-enhanced 3D ^{15}N -separated TOCSY-HSQC (Wijmenga et al., 1996) experiment was recorded on ^{15}N -/ ^{13}C -labeled holoflavodoxin using a 47-ms DIPSI-3 sequence (Shaka et al., 1988) of 8.7 kHz for ^1H - ^1H TOCSY transfer.

$^3J_{\text{HN-Ha}}$ coupling constants were determined from a 3D HNHA (Vuister & Bax, 1993) experiment, employing a correction factor of 1.2. Water was presaturated during the relaxation delay because no gradients were implemented in the pulse sequence. Furthermore, the proton carrier frequency was positioned in the center of the amide region, except during presaturation and acquisition in which its position coincided with the water frequency.

Additional acquisition parameters for the multidimensional NMR experiments are provided in Table 1.

Data processing and analysis

NMR data were processed on Silicon Graphics Indigo II workstations using Felix version 2.3 (Biosym Technologies, San Diego, California). Fids (of the acquisition dimension) were multiplied by a Gaussian function and zero-filled to 1K prior to Fourier transformation. In all indirect dimensions, data were apodized using a 90° shifted sine-bell squared window function and zero-filled to the next power of 2 prior to Fourier transformation. When necessary, a FLATT baseline correction was applied to the transformed data (Güntert & Wüthrich, 1992). The spectra were analyzed using the program XEASY (ETH, Zurich, Switzerland; Bartels et al. 1995). The ^1H chemical shifts were referenced using internal TSP as a standard, and pH-corrected values are reported here in ppm relative to DSS. ^{15}N and ^{13}C chemical shifts were referenced indirectly using the consensus Ξ ratios of 0.101329118 and 0.251449530 for ^{15}N and ^{13}C , respectively (Wishart et al., 1995). A consensus CSI for assigning protein secondary structure was calculated using the Chemical Shift Index program (Wishart et al., 1992; Wishart & Sykes, 1994). Figure 4 was made with help of the program Tablenoe written by Bruno Kieffer (Strasbourg, France).

Hydrogen exchange experiments

A 500- μL sample of uniformly ^{15}N -labeled holoflavodoxin in 150 mM potassium pyrophosphate pH* 6.0 was lyophilized, reconstituted in 99.9% $^2\text{H}_2\text{O}$ (Isotec Inc., USA), and centrifuged to remove aggregates. The final sample contained 4.3 mM holoflavodoxin and the pH* of the sample was 6.2. The first gradient-enhanced ^1H - ^{15}N HSQC experiment, which was sensitivity optimized by employing a selective Gaussian water flip-back pulse (Palmer et al., 1991; Kay et al., 1992; Stonehouse et al., 1994), was started 10 min after initiation of exchange. The spectra were acquired at 303 K on a Bruker AMX 500 spectrometer over a 42-h period. Data were acquired with 512 complex points in t_2 and with 128 complex points in t_1 , spectral widths were 8,065 Hz and 1,863 Hz in t_2 and t_1 , respectively. Each individual experiment lasted about 11 min. The data were zero-filled to obtain a final point-to-point resolution of 2 Hz in F_2 and 1 Hz in F_1 , respectively, apodized using a Gaussian multiplication in t_2 and a 90° shifted sine-bell squared window function in t_1 , respectively, Fourier transformed, and baseline corrected in both dimensions using the FLATT procedure (Güntert & Wüthrich, 1992).

Hydrogen exchange data analysis

Peak intensities were measured in XEASY (Bartels et al., 1995) as the maximum intensity of each individual cross peak in an ^1H - ^{15}N HSQC spectrum. The time-dependent peak intensities obtained were subsequently fitted to a single exponential decay function

(Equation 9) using KaleidaGraph version 2.1.3 (Abelbeck, Synergy Software, Reading, Pennsylvania) to determine k_{ex} :

$$I(t) = I(\infty) + I(0)\exp(-k_{ex} * t). \quad (9)$$

The variable time t comprises the time between the addition of $^2\text{H}_2\text{O}$ to the lyophilized holoflavodoxin and the beginning of each individual $^1\text{H}-^{15}\text{N}$ HSQC experiment, $I(0)$ is the peak intensity at time zero, and $I(\infty)$ is the peak intensity at the infinity time point. At least 10 exchange data points per individual amide proton were used. A least-squares fit of these exchange data to Equation 9 gave k_{ex} and the corresponding standard error value. Standard errors obtained in this way were generally less than 5% of the k_{ex} values obtained. However, the standard errors for k_{ex} values ranging from 10^{-2} s^{-1} to 10^{-4} s^{-1} were between 10% and 20%. The latter is due to the limited number of data points that had a cross peak intensity above noise level. For amide protons that did not exchange completely within 42 h and for which the infinity time-point was not well-determined, the decay curve was fitted using a final intensity of zero.

ΔG_{op}^{app} values were determined from the observed rate constants, k_{ex} , and the intrinsic chemical exchange rates, k_{int} , using Equation 6. The intrinsic exchange rates were calculated using free peptide exchange rates, which were corrected for the effects of the local amino acid sequence and calibrated for the pH and the temperature of our exchange experiment, as described by Bai et al. (1993).

Supplementary material in electronic appendix

The chemical shifts of the ^1H , ^{15}N , and ^{13}C backbone and the $^1\text{H}^\beta$ and $^{13}\text{C}^\beta$ resonances of *A. vinelandii* holoflavodoxin II (in 90% H_2O /10% $^2\text{H}_2\text{O}$, 150 mM potassium pyrophosphate, pH* 6.0, 303 K) are given in Table 1. Table 2 gives the logarithm of the amide proton exchange rates and the calculated apparent free energies ΔG_{op}^{app} (298 K) for *A. vinelandii* holoflavodoxin II in 150 mM potassium pyrophosphate, pH* 6.2, 303 K.

Acknowledgments

We thank Frank Vergeldt for assistance with computers, Sjaak Peelen for modifying Felix macros, Lars Ridder for his help in awk-programming, and Jos Buijs for stimulating and helpful discussions. The 600-MHz NMR data were acquired at the SON/NWO National HF-NMR Facility in Nijmegen, The Netherlands. We collaborated with Sybren Wijmenga to record and modify some of the reported 3D NMR experiments. We thank B. Kieffer (Strasbourg, France) for sharing his program Tablenoe with the NMR community. The research of C.P.M. van Mierlo has been made possible by a fellowship of the Royal Netherlands Academy of Arts and Sciences.

References

- Archer SJ, Ikura M, Torchia DA, Bax A. 1991. An alternative 3D NMR technique for correlating backbone ^{15}N with side chain H^β resonances in larger proteins. *J Magn Reson* 95:636–641.
- Bai Y, Milne JS, Mayne L, Englander SW. 1993. Primary structure effects on peptide group hydrogen exchange. *Proteins Struct Funct Genet* 17:75–86.
- Balbach J, Forge V, Lau WS, van Nuland NAJ, Brew K, Dobson CM. 1996. Protein folding monitored at individual residues during a two-dimensional NMR experiment. *Science* 274:1161–1163.
- Balbach J, Forge V, van Nuland NAJ, Winder SL, Hore PJ, Dobson CM. 1995. Following protein folding in real time using NMR spectroscopy. *Nature Struct Biol* 2:865–870.
- Bartels C, Xia T, Billeter M, Güntert P, Wüthrich K. 1995. The program XEASY for computer-supported NMR spectral analysis of biological macromolecules. *J Biomol NMR* 5:1–10.
- Bowie JU, Clarke ND, Pabo CO, Sauer RT. 1990. Identification of protein folds: Matching hydrophobicity patterns of sequence sets with solvent accessibility patterns of known structures. *Proteins Struct Funct Genet* 7:257–264.
- Bruix M, Muñoz V, Campos-Olivas R, Del Bosque JR, Serrano L, Rico M. 1997. Characterisation of the isolated Che Y C-terminal fragment (79–129)—Exploring the structure/stability/folding relationships of the α/β parallel protein Che Y. *Eur J Biochem* 243:384–392.
- Cavanagh J, Rance M. 1990. Sensitivity improvement in isotropic mixing (TOCSY) experiments. *J Magn Reson* 88:72–85.
- Cavanagh J, Rance M. 1992. Suppression of cross-relaxation effects in TOCSY spectra via a modified DIPSI-2 mixing sequence. *J Magn Reson* 96:670–678.
- Clubb RT, Thanabal V, Osborne C, Wagner G. 1991. ^1H and ^{15}N resonance assignments of oxidized flavodoxin from *Anacystis nidulans* with 3D NMR. *Biochemistry* 30:7718–7730.
- Clubb RT, Thanabal V, Wagner G. 1992. A constant-time three-dimensional triple-resonance pulse scheme to correlate intraresidue $^1\text{H}^\alpha$, ^{15}N , and $^{13}\text{C}'$ chemical shifts in $^{15}\text{N}, ^{13}\text{C}$ -labeled proteins. *J Magn Reson* 97:213–217.
- Englander SW, Kallenbach NR. 1984. Hydrogen exchange and structural dynamics of proteins and nucleic acids. *Q Rev Biophys* 16:521–655.
- Englander SW, Mayne L. 1992. Protein folding studied using hydrogen-exchange labeling and two-dimensional NMR. *Annu Rev Biophys Biomol Struct* 21:243–265.
- Englander SW, Sosnick TR, Englander JJ, Mayne L. 1996. Mechanisms and uses of hydrogen exchange. *Curr Opin Struct Biol* 6:18–23.
- Frenkel T, Bauer C, Carr MD, Birdsall B, Feeney J. 1990. HMQC-NOESY-HMQC, a three-dimensional NMR experiment which allows detection of nuclear Overhauser effects between protons with overlapping signals. *J Magn Reson* 90:420–425.
- Fukuyama K, Matsubara H, Rogers LJ. 1992. Crystal structure of oxidized flavodoxin from a red alga *Chondrus crispus* refined at 1.8 Å resolution—Description of the flavin mononucleotide binding site. *J Mol Biol* 225:775–789.
- Grandori R, Carey J. 1994. Six new candidate members of the α/β twisted open-sheet family detected by sequence similarity to flavodoxin. *Protein Sci* 3:2185–2193.
- Grzesiek S, Bax A. 1992a. Improved 3D triple-resonance NMR techniques applied to a 31 kDa protein. *J Magn Reson* 96:432–440.
- Grzesiek S, Bax A. 1992b. An efficient experiment for sequential backbone assignment of medium-sized isotopically enriched proteins. *J Magn Reson* 99:201–207.
- Grzesiek S, Bax A. 1992c. Correlating backbone amide and side chain resonances in larger proteins by multiple relayed triple resonance NMR. *J Am Chem Soc* 114:6291–6293.
- Grzesiek S, Bax A. 1993. Amino acid type determination in the sequential assignment procedure of uniformly $^{13}\text{C}/^{15}\text{N}$ -enriched proteins. *J Biomol NMR* 3:185–204.
- Güntert P, Wüthrich K. 1992. FLATT—A new procedure for high-quality baseline correction of multidimensional NMR spectra. *J Magn Reson* 96:403–407.
- Hvidt A, Nielsen SO. 1966. Hydrogen exchange in proteins. *Adv Protein Chem* 21:287–386.
- Ikura M, Bax A, Clore GM, Gronenborn AM. 1990. Detection of nuclear Overhauser effects between degenerate amide proton resonances by heteronuclear three-dimensional nuclear magnetic resonance spectroscopy. *J Am Chem Soc* 112:9020–9022.
- Jahnke W, Kessler H. 1994. Enhanced sensitivity of rapidly exchanging amide protons by improved phase cycling and the constructive use of radiation damping. *J Biomol NMR* 4:735–740.
- Jeng MF, Dyson HJ. 1995. Comparison of the hydrogen-exchange behavior of reduced and oxidized *Escherichia coli* thioredoxin. *Biochemistry* 34:611–619.
- Kay LE, Keifer P, Saarinen T. 1992. Pure absorption gradient enhanced heteronuclear single quantum correlation spectroscopy with improved sensitivity. *J Am Chem Soc* 114:10663–10665.
- Linderstrøm-Lang K. 1955. Deuterium exchange between peptides and water. *Chem Soc (London) Spec Publ* 2:1–20.
- López-Hernández E, Cronet P, Serrano L, Muñoz V. 1997. Folding kinetics of Che Y mutants with enhanced native α -helix propensities. *J Mol Biol* 266:610–620.
- López-Hernández E, Serrano L. 1996. Structure of the transition state for folding of the 129 aa protein CheY resembles that of a smaller protein, Cl-2. *Folding & Design* 1:43–55.
- Ludwig ML, Luschinsky CL. 1992. Structure and redox properties of clostridial flavodoxin. In: Müller F, ed. *Chemistry and biochemistry of flavoenzymes*, vol 3. Boca Raton, Florida: CRC Press. pp 427–466.

- Marion D, Driscoll PC, Kay LE, Wingfield PT, Bax A, Gronenborn AM, Clore GM. 1989a. Overcoming the overlap problem in the assignment of ^1H NMR spectra of larger proteins by use of three-dimensional heteronuclear ^1H - ^{15}N Hartmann-Hahn-multiple quantum coherence and nuclear Overhauser-multiple quantum coherence spectroscopy: Application to interleukin 1 β . *Biochemistry* 28:6150–6156.
- Marion D, Ikura M, Tschudin R, Bax A. 1989b. Rapid recording of 2D NMR spectra without phase cycling. Application to the study of hydrogen exchange in proteins. *J Magn Reson* 85:393–399.
- Mayhew SG, Tollin G. 1992. General properties of flavodoxins. In: Müller F, ed. *Chemistry and biochemistry of flavoenzymes, vol 3*. Boca Raton, Florida: CRC Press. pp 389–426.
- Orengo CA, Jones DT, Thornton JM. 1994. Protein superfamilies and domain superfolds. *Nature* 372:631–634.
- Palmer AG III, Cavanagh J, Wright PE, Rance M. 1991. Sensitivity improvement in proton-detected two-dimensional heteronuclear correlation NMR spectroscopy. *J Magn Reson* 93:151–170.
- Patt SL. 1992. Single- and multiple-frequency-shifted laminar pulses. *J Magn Reson* 96:94–102.
- Peelen S, Wijmenga SS, Erbel PJA, Robson RL, Eady RR, Vervoort J. 1996. Possible role of a short extra loop of the long-chain flavodoxin from *Azotobacter chroococcum* in electron transfer to nitrogenase: Complete ^1H , ^{15}N and ^{13}C backbone assignments and secondary solution structure of the flavodoxin. *J Biomol NMR* 7:315–330.
- Pueyo JJ, Curley GP, Mayhew SG. 1996. Kinetics and thermodynamics of the binding of riboflavin, riboflavin 5'-phosphate and riboflavin 3',5'-bisphosphate by apoflavodoxins. *Biochem J* 313:855–861.
- Remerowski ML, Domke T, Groenewegen A, Pepermans HAM, Hilbers CW, van de Ven FJM. 1994. ^1H , ^{13}C and ^{15}N NMR backbone assignments and secondary structure of the 269-residue protease subtilisin 309 from *Bacillus lentus*. *J Biomol NMR* 4:257–278.
- Sayle RA, Milner-White EJ. 1995. RasMol: Biomolecular graphics for all. *Trends Biochem Sci* 20:374–376.
- Shaka AJ, Barker PB, Freeman R. 1985. Computer-optimized decoupling scheme for wideband applications and low-level operation. *J Magn Reson* 64:547–552.
- Shaka AJ, Lee CJ, Pines A. 1988. Iterative schemes for bilinear operators; application to spin decoupling. *J Magn Reson* 77:274–293.
- Shortle DR. 1996. Structural analysis of non-native states of proteins by NMR methods. *Curr Opin Struct Biol* 6:24–30.
- Steenisma E, Heering HA, Hagen WR, van Mierlo CPM. 1996. Redox properties of wild-type, Cys69Ala, and Cys69Ser *Azotobacter vinelandii* flavodoxin II as measured by cyclic voltammetry and EPR spectroscopy. *Eur J Biochem* 235:167–172.
- Stockman BJ, Euvrard A, Kloosterman DA, Scanhill TA, Swenson RP. 1993. ^1H and ^{15}N resonance assignments and solution secondary structure of oxidized *Desulfovibrio vulgaris* flavodoxin determined by heteronuclear three-dimensional NMR spectroscopy. *J Biomol NMR* 3:133–149.
- Stockman BJ, Richardson TE, Swenson RP. 1994. Structural changes caused by site-directed mutagenesis of tyrosine-98 in *Desulfovibrio vulgaris* flavodoxin delineated by ^1H and ^{15}N NMR spectroscopy: Implications for redox potential modulation. *Biochemistry* 33:15298–15308.
- Stockman BJ, Westler WM, Mooberry ES, Markley JL. 1988. Flavodoxin from *Anabaena* 7120: Uniform nitrogen-15 enrichment and hydrogen-1, nitrogen-15, and phosphorus-31 NMR investigations of the flavin mononucleotide binding site in the reduced and oxidized states. *Biochemistry* 27:136–142.
- Stonehouse J, Shaw GL, Keeler J, Laue ED. 1994. Minimizing sensitivity losses in gradient-selected ^{15}N - ^1H HSQC spectra of proteins. *J Magn Reson A* 107:178–184.
- Swenson RP, Krey GD. 1994. Site-directed mutagenesis of tyrosine-98 in the flavodoxin from *Desulfovibrio vulgaris* (Hildenborough): Regulation of oxidation-reduction properties of the bound FMN cofactor by aromatic, solvent, and electrostatic interactions. *Biochemistry* 33:8505–8514.
- Swindells MB. 1993. Classification of doubly wound nucleotide binding topologies using automated loop searches. *Protein Sci* 2:2146–2153.
- Tanaka M, Haniu M, Yasunobu KT, Yoch DC. 1977. Complete amino acid sequence of azotoflavin, a flavodoxin from *Azotobacter vinelandii*. *Biochemistry* 16:3525–3537.
- Thorneley RNF, Ashby GA, Drummond MH, Eady RR, Hughes DL, Ford G, Harrison PM, Shaw A, Robson RL, Kazlauskaitė J, Hill HAO. 1994. Flavodoxins and nitrogen fixation—Structure, electrochemistry and post-translational modification by coenzyme A. In: Yagi K, ed. *Flavins and flavoproteins 1993*. Berlin: Walter de Gruyter & Co. pp 343–354.
- Tollin G, Edmondson DE. 1980. Purification and properties of flavodoxins. *Methods Enzymol* 69:392–406.
- van Mierlo CPM, Lijnzaad P, Vervoort J, Müller F, Berendsen HJC, De Vlieg J. 1990a. Tertiary structure of two-electron reduced *Megasphaera elsdenii* flavodoxin and some implications, as determined by two-dimensional ^1H NMR and restrained molecular dynamics. *Eur J Biochem* 194:185–198.
- van Mierlo CPM, Steensma E, van Dongen WMAM, van Berkell WJH. 1997. NMR studies on apoflavodoxin II from *Azotobacter vinelandii*. In: Stevenson KJ, Massey V, Williams CH Jr, eds. *Flavins and flavoproteins 1996*. Calgary: University of Calgary Press. pp 449–452.
- van Mierlo CPM, Vervoort J, Müller F, Bacher A. 1990b. A two-dimensional ^1H NMR study on *Megasphaera elsdenii* flavodoxin in the reduced state: Sequential assignments. *Eur J Biochem* 187:521–541.
- Vuister GW, Bax A. 1993. Quantitative J correlation: A new approach for measuring homonuclear three-bond $J(\text{H}^1\text{H}^2)$ coupling constants in ^{15}N -enriched proteins. *J Am Chem Soc* 115:7772–7777.
- Wagner G, Wüthrich K. 1979. Correlation between the amide proton exchange rates and the denaturation temperatures in globular proteins related to the basic pancreatic trypsin inhibitor. *J Mol Biol* 130:31–37.
- Wijmenga SS, van Mierlo CPM, Steensma E. 1996. Doubly sensitivity-enhanced 3D TOCSY-HSQC. *J Biomol NMR* 8:319–330.
- Wishart DS, Bigam CG, Yao J, Abildgaard F, Dyson HJ, Oldfield E, Markley JL, Sykes BD. 1995. ^1H , ^{13}C , and ^{15}N chemical shift referencing in biomolecular NMR. *J Biomol NMR* 6:135–140.
- Wishart DS, Sykes BD. 1994. The ^{13}C chemical-shift index: A simple method for the identification of protein secondary structure using ^{13}C chemical-shift data. *J Biomol NMR* 4:171–180.
- Wishart DS, Sykes BD, Richards FM. 1992. The chemical shift index: A fast and simple method for the assignment of protein secondary structure through NMR spectroscopy. *Biochemistry* 31:1647–1651.
- Woodward CK. 1994. Hydrogen exchange rates and protein folding. *Curr Opin Struct Biol* 4:112–116.
- Wüthrich K. 1986. *NMR of proteins and nucleic acids*. New York: Wiley.
- Zhou Z, Swenson RP. 1995. Electrostatic effects of surface acidic amino acid residues on the oxidation-reduction potentials of the flavodoxin from *Desulfovibrio vulgaris* (Hildenborough). *Biochemistry* 34:3183–3192.
- Zhou Z, Swenson RP. 1996a. Evaluation of the electrostatic effect of the 5'-phosphate of the flavin mononucleotide cofactor on the oxidation-reduction potentials of the flavodoxin from *Desulfovibrio vulgaris* (Hildenborough). *Biochemistry* 35:12443–12454.
- Zhou Z, Swenson RP. 1996b. The cumulative electrostatic effect of aromatic stacking interactions and the negative electrostatic environment of the flavin mononucleotide binding site is a major determinant of the reduction potential for the flavodoxin from *Desulfovibrio vulgaris* (Hildenborough). *Biochemistry* 35:15980–15988.